Effect of Diaphragm Flexibility on the Dynamic Behaviour of Unreinforced Masonry Walls in Out-of-Plane Bending

R. Gabellieri, P.P. Diotallevi & L. Landi
Department of Civil, Environmental and Materials Engineering - DICAM,
University of Bologna, Bologna, Italy

SUMMARY:
This paper investigates the dynamic behaviour of the external walls of unreinforced masonry historic buildings with flexible diaphragms subjected to out-of-plane bending. The influence of diaphragms flexibility on the displacement capacity and demand of walls in out-of-plane bending has been studied by means of dynamic analyses with a simplified two-degrees-of-freedom model (2DOF). The wall has been modelled as an assemblage of two rigid bodies connected by an intermediate hinge and restrained at the top by a spring: the damping has been modelled through the introduction of the coefficient of restitution. The equations of motion of the 2DOF system have been derived and integrated in the time domain. Dynamic analyses of a set of walls with Gaussian impulse and recorded accelerogram inputs have been performed in order to compare the response of the simply supported wall with the one of the wall with an elastic spring at the top.

Keywords: Out-of-Plane Bending; Unreinforced Masonry; Dynamic Analysis; Flexible Diaphragms

1. INTRODUCTION

The observation of the damages produced by earthquakes on historical unreinforced masonry buildings pointed out that out-of-plane collapses of the external walls are frequent and very dangerous even in terms of loss of human lives. Historical buildings are in fact characterized by weak connections between the different structural elements and tend therefore to exhibit local collapses before global ones. During earthquakes single parts separate from the rest of the building, often behaving as quite independent structural elements. The study of the behaviour of such mechanisms is then essential and has been undertaken by many authors in the recent years. Different approaches have been proposed, like static, kinematic or dynamic analyses, elasto-plastic, no-tension or rigid models but the experimental tests are still relatively few and have been concentrated on the simplest failure modes because of their simpler reproducibility and interpretation (parapet wall or simply supported wall). Housner work (Housner, 1963) represented the basis of the dynamic studies on the wall as a single rigid block: other studies followed his hypotheses and delved into this topic, but only recently some analytical and experimental studies (Doherty, 2000; Doherty et al., 2002; Griffith et al., 2003; Griffith et al., 2004; Lam et al., 2003; Sorrentino, 2003; Sorrentino, 2008) highlighted the necessity of dynamic analysis in order to understand the real behaviour of walls in out-of-plane bending and to assess, without an over conservative approach, the vulnerability against earthquake action. They pointed out the fact that out-of-plane failures of walls are caused essentially by an excessive displacement demand rather than force or acceleration demand and that static methods, focused on the comparison between forces and resistance, cannot then catch some specific aspects related to the dynamic behaviour. Quite all the past works considered simplified hypotheses about the interaction of the wall with the rest of the building, assuming diaphragms as rigid and reducing therefore the complexity of the dynamic problem and the number of the degrees of freedom. The path of the seismic action from the ground to the out-of-plane walls implies a filtering effect of the shear walls and diaphragm response: when the diaphragms cannot be considered as rigid, like in most historical buildings, the inputs to the out-of-plane walls at adjacent floors have different amplitude, phase and

frequency content. In this case it is necessary to consider multiple-degrees-of-freedom instead of the usual single-degree model. There are really few studies (Simsir, 2004) that take directly into account the influence of flexibility of diaphragms on the displacement capacity and demand. Extending some formulations proposed by other authors (Doherty, 2000; Sorrentino, 2003; Simsir, 2004) a simplified 2DOF model has been developed to analyse the dynamic out-of-plane behaviour of a single wall with the hypothesis of flexible diaphragm. The equations of motion of the wall have been derived and an algorithm for their numerical integration has been developed: the main results are presented.

2. MODEL DESCRIPTION

A simplified 2DOF model has been developed to analyse the dynamic out-of-plane behaviour of a single wall, with an intermediate hinge and an elastic spring at the top. The wall, as shown in Fig. 1.1, is modelled as an assemblage of two rigid bodies, a lower and an upper part, each one free to rotate around the intermediate hinge.
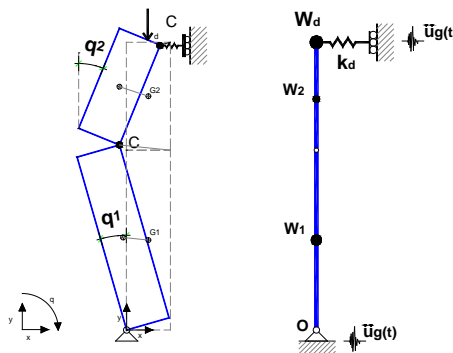

Figure 2.1 2DOF model of the wall in out-of-plane bending

In Fig. 2.1 W_1 and W_2 are the weights of the lower and upper part of the wall, W_d is the overburden load from the diaphragm, K_d is the translational stiffness of the spring at the top, that simulates the in-plane stiffness of the upper diaphragm and is considered perfectly elastic, q_1 e q_2 are the rotations, respectively of the lower and the upper portion of the wall related to the vertical axis, that have been assumed as independent variables. The intermediate hinge has been assumed at the mid-height of the wall and the load W_d is supposed to be applied at the middle of the thickness, in order to reproduce the hypotheses made by Doherty in his study on the simply supported wall (Doherty, 2000) and to compare the results obtained by Doherty with the ones of the present study.

3. EQUATIONS OF MOTION

The equations of motion of the 2DOF system have been derived by applying Lagrange equations, considering the kinetic energy due to the translation of the masses and to the rotation of the two parts of the wall around the respective centroids and the potential energy due to the translational spring at the top and to the contribution of the gravitational loads. The above mentioned quantities have been calculated with the assumption of small displacements.

3.1. Geometric possible configurations

The equations of motion are highly non linear because of the sudden change of the point of rotation at the base and at the intermediate hinge. There are four different conditions described by four corresponding sets of equations (see Fig. 3.1): the passage from one condition to another is determined by an impact at the bottom or at the intermediate hinge associated with the change of the centre of rotation (see Fig. 3.2).
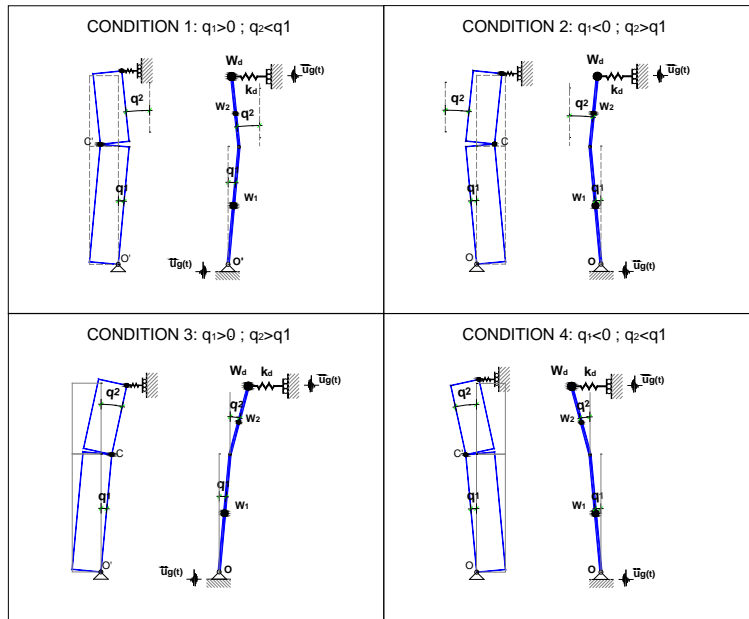
Figure 3.1 2DOF model of the wall in out-of-plane bending

Every time q_1 passes through the zero, there is an impact at the bottom and a change of the centre of rotation (O to O' or O' to O): similarly, every time $q_1 = q_2$, there is an impact at the intermediate hinge and a change of the centre of rotation (C to C' or C' to C).
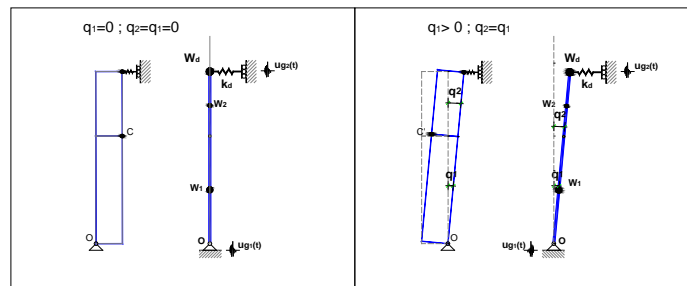

Figure 3.2 Impacts at the bottom hinge (left, q_1=0) and at the intermediate hinge (right, $q_1 = q_2$)

3.2. Energy dissipation

Following the Housner model (Housner, 1963), the dissipation of energy is concentrated at every impact at the base of the wall and is modelled through the introduction of the coefficient of restitution, $e_r < 1$, that relates the velocities after each impact to those immediately before, reproducing the loss of kinetic energy at each impact.

3.3. Equations of motion

Assuming h for the total height of the wall, g for the gravity acceleration, $W_1 = W_2$, because of the position of the intermediate hinge at the mid-height of the wall, and the clockwise rotations as positive, the equations of motion are:

$$\begin{bmatrix} m_{11} & m_{12} \\ m_{21} & m_{22} \end{bmatrix} \cdot \begin{bmatrix} \ddot{q}_1 \\ \ddot{q}_2 \end{bmatrix} + \begin{bmatrix} k_{11} & k_{12} \\ k_{21} & k_{22} \end{bmatrix} \cdot \begin{bmatrix} q_1 \\ q_2 \end{bmatrix} = \begin{bmatrix} p'_{eff,1}(t) + A_i \\ p'_{eff,2}(t) + B_i \end{bmatrix}$$

(3.1)

The coefficients of the mass matrix are reported in Eqn. 3.2:

$$\begin{cases} m_{11} = \left[\dfrac{W_1}{3} + \dfrac{W_d}{4}\right] \cdot \dfrac{h^2}{g} \\[3mm] m_{12} = m_{21} = \left[\dfrac{W_1}{8} + \dfrac{W_d}{4}\right] \cdot \dfrac{h^2}{g} \\[3mm] m_{22} = \left[\dfrac{W_1}{12} + \dfrac{W_d}{4}\right] \cdot \dfrac{h^2}{g} \end{cases}$$
(3.2)

The coefficients of the stiffness matrix are reported in Eqn. 3.3:

$$\begin{cases} k_{11} = \left[\dfrac{K_d \cdot h^2}{4} - \dfrac{3}{4} \cdot W_1 \cdot h - W_d \cdot \dfrac{h}{2}\right] \\[3mm] k_{12} = k_{21} = \dfrac{K_d \cdot h^2}{4} \\[3mm] k_{22} = \left[\dfrac{K_d \cdot h^2}{4} - W_1 \cdot \dfrac{h}{4} - W_d \cdot \dfrac{h}{2}\right] \end{cases}$$
(3.3)

The terms $p_{eff,1}(t)$ and $p_{eff,2}(t)$ represent the contribution due to the ground acceleration. They are reported in Eqn. 3.4:

$$\begin{cases} p'_{eff,1}(t) = -\ddot{u}_g \cdot \left[-3 \cdot W_1 - 2 \cdot W_d\right] \cdot \dfrac{h}{4 \cdot g} \\[3mm] p'_{eff,2}(t) = -\ddot{u}_g \cdot \left[-W_2 - 2 \cdot W_d\right] \cdot \dfrac{h}{4 \cdot g} \end{cases}$$
(3.4)

The terms A_i and B_i in Eqn. 3.1 are different in the four conditions: they are expressed in Eqn. 3.5, 3.6, 3.7, 3.8.
Condition 1 ($q_1 > 0$ and $q_2 < q_1$):

$$\begin{cases} A_1 = -\dfrac{3 \cdot W_1}{2} \cdot b - W_d \cdot b \\[3mm] B_1 = \dfrac{W_1}{2} \cdot b + W_d \cdot \dfrac{b}{2} \end{cases}$$
(3.5)

Condition 2 ($q_1 < 0$ and $q_2 > q_1$):

$$\begin{cases} A_1 = -\dfrac{3 \cdot W_1}{2} \cdot b - W_d \cdot b \\[3mm] B_1 = \dfrac{W_1}{2} \cdot b + W_d \cdot \dfrac{b}{2} \end{cases}$$
(3.6)

Condition 3 ($q_1 > 0$ and $q_2 > q_1$):

$$\begin{cases} A_2 = +\dfrac{3 \cdot W_1}{2} \cdot b + W_d \cdot b \\[3mm] B_2 = -\dfrac{W_1}{2} \cdot b - W_d \cdot \dfrac{b}{2} \end{cases}$$
(3.7)

Condition 4 ($q_1 < 0$ and $q_2 < q_1$):

$$\begin{cases} A_4 = +\dfrac{W_1}{2} \cdot b \\[2ex] B_4 = +\dfrac{W_1}{2} \cdot b + W_d \cdot \dfrac{b}{2} \end{cases}$$

(3.8)

4. NUMERICAL ALGORITHM

An algorithm for the numerical integration of the sets of the equations of motion in the time domain has been developed: a variable step size Runge-Kutta integration method of 4th-5th order, implemented in Matlab ODE-suite ODE45, has been used. A local error control has been performed at each step of the numerical integration: sufficiently small values of relative tolerance *RelTol* and absolute tolerance *AbsTol* have been assumed (*RelTol*=10[-5] and *AbsTol*=10[-10]). The strong nonlinearity of the set of equations of motion is produced by the sudden change of the sign of the resisting moment of the weights W_1 and W_2 and of W_d about the effective centre of rotation at the bottom and intermediate hinges, corresponding to the sudden change of the position of the hinge at every impact.

$$M_{q_1} = \left[\frac{3}{4} \cdot W_1 \cdot h + W_d \cdot \frac{h}{2} \right] \cdot q_1 + A_i$$

(4.1)

$$M_{q_2} = \left[\frac{W_1}{4} \cdot h + W_d \cdot \frac{h}{2} \right] \cdot q_2 + B_i$$

(4.2)

Eqn. 4.1 and Eqn. 4.2 present the expression of M_{q1} and M_{q2}: M_{q1} is the resisting moment about the bottom hinge O or O' (depending on the actual condition) of the self weight W_1 of the lower part of the wall and of the weights $W_2=W_1$ and W_d transferred from the upper to the lower part of the wall at the intermediate hinge C or C'; M_{q2} is the resisting moment about the intermediate hinge C or C'(depending on the actual condition) of the weights W_2 and W_d. A_i and B_i are presented in Eqn. 3.5, Eqn. 3.6, Eqn. 3.7 and Eqn. 3.8 and represent the resisting moments M_{q1} and M_{q2} when the independent variables q_1 and q_2 are zero.

Fig. 4.1 shows the diagrams of M_{q1} in the 4 conditions (green and red continuous lines): the blue dotted line represents the diagram of M_{q1} in the hypothesis of rigid behaviour of the wall. Similarly to what proposed in Doherty studies (Doherty, 2000), a finite stiffness instead of an infinite stiffness at $q_1=0$ is assumed, so that the two purple and yellow lines describe the transition from one condition to another at $q_1=0$. The algorithm follows then these lines instead of the blue ones of the rigid behaviour. The parameters $-D_{12,1}$, $-D_{34,1}$, $D_{34,1}$, $D_{12,1}$ are the values of q_1 at the intersections of the diagrams of M_{q1} in the 4 conditions with the line of finite stiffness. Transitions from condition 1 to 4 or from 4 to 1 and from 2 to 3 or from 3 to 2 take place when an impact at the intermediate hinge occurs ($q_1=q_2$) and are represented by the vertical black dotted lines.
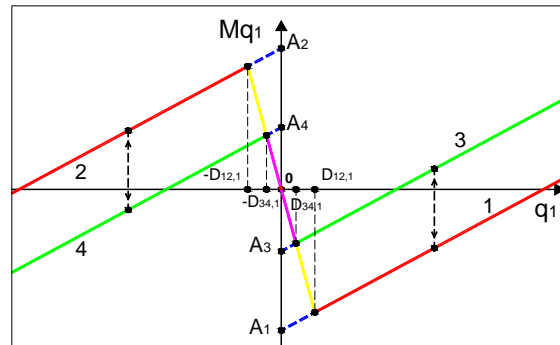

Figure 4.1 Resisting moment M_{q1} in the 4 conditions

Fig. 4.2 shows the diagrams of M_{q2} in the 4 conditions (red continuous lines): the couples of conditions 1 and 4, 2 and 3 have the same diagram. Similarly to the diagram of Fig. 4.1 an initial finite stiffness is assumed (purple dotted line). The parameters $-D_{12,2}$, $D_{12,2}$ are the values of q_2 at the intersections of the diagrams of M_{q2} in the 4 conditions with the line of finite stiffness. Transitions from conditions 1 or 4 to conditions 2 or 3 or from conditions 2 or 3 to conditions 1 or 4, corresponding to an impact at the intermediate hinge ($q_1=q_2$), are represented by the vertical black dotted lines, while transitions at $q_1=0$ do not cause any jump in the diagram.
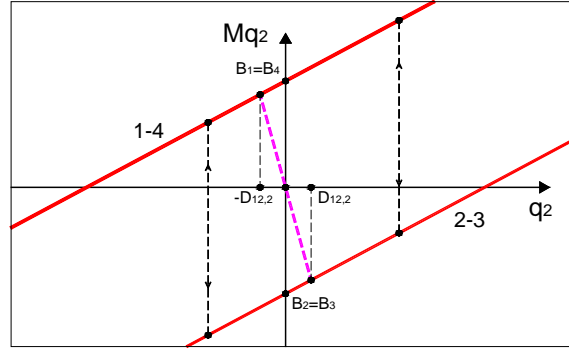

Figure 4.2 Resisting moment M_{q2} in the 4 conditions

Defined the initial conditions $q_1(0)$, $q_2(0)$, $\dot{q}_1(0)$, $\dot{q}_2(0)$ the numerical algorithm integrates the equations of motion of the Eqn. 3.1 until the first event: the algorithm can detect the events at the target values of q_1 and q_2: the integration stops when the variable q_1 assumes the values $-D_{12,1}$, $-D_{34,1}$, 0, $D_{34,1}$, $D_{12,1}$ or when the variable q_2 assumes the values $-D_{12,2}$, $D_{12,2}$ or when $q_1 = q_2$. State variables identify the condition corresponding to each time step: the value of these variables at the event defines the condition before the event and allows the algorithm to decide which condition to assume afterwards and which line to follow in Fig. 3.1 and 3.2. Except for the impact for $q_1=0$, the values of the rotations q_1 and q_2 and the corresponding angular velocities after every event are the same detected at the event. These are the new initial conditions of the differential equations that the algorithm assumes in order to integrate the appropriate equations, depending on the effective initial geometrical configuration of the wall. For $q_1=0$, the rotations after the impact are the same as the ones before the impact, while the angular velocities of the lower and upper part of the wall are reduced by the restitution coefficient $e_r<1$.

5. RESULTS

An algorithm for the integration of the equations of motion of the semi-rigid 1DOF model proposed by Doherty (Doherty, 2000) has been implemented to validate the numerical strategy used in the present work and to compare Doherty's results to the ones obtained with the 2DOF model in the case of a very high value of stiffness of the top spring: in that case the top and bottom absolute displacements of the wall tend to be equal and in phase and the behaviour of the 2DOF model should coincide with the one of the simpler 1DOF model. The experimental and analytical results obtained by Doherty showed a good agreement with the 1DOF model developed in the present work. Dynamic analyses with Gaussian and recorded accelerogram inputs have been performed on a set of walls, varying the values of the stiffness K_d at the top and studying its influence on the displacement demand. A coefficient of restitution $e_r=0.86$ is used both for the 1DOF and for the 2DOF model.

5.1. Set of walls

A set of 3 walls with different characteristics, in terms of maximum resisting force and ultimate displacement in the hypothesis of rigid behaviour (see Table 5.1 and Fig. 5.1) has been considered.

Table 5.1. Set of considered walls

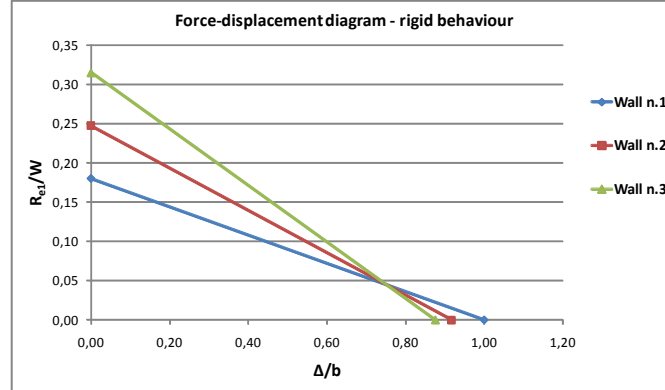| Wall	b	h	Ψ	W	R_{el}	Δ_u	F0/W	Δ_u/b
	[m]	[m]	[-]	[KN/m]	[KN/m]	[m]	[-]	[-]
1	0,15	2,5	0	6,622	1,192	0,150	0,180	1,000
2	0,15	2,5	0,5	6,622	1,639	0,138	0,248	0,917
3	0,15	2,5	1	6,622	2,086	0,131	0,315	0,875

Figure 5.1 Adimensional force-displacement curves of the 3 walls

In Table 5.1 *b* is the thickness, *h* is the height, *W* is the self weight of the wall, Ψ is the ratio between W_d and W_l, R_{el} is the rigid threshold resistance and Δ_u is the ultimate displacement, calculated following Doherty formulation (Doherty, 2000; Doherty et al., 2002).

5.2. Semi-rigid 1DOF model

The semi-rigid 1DOF model proposed by Doherty has been implemented. Fig. 5.2 shows the mid-height acceleration-displacement curve for the rigid (blue dotted line) and semi-rigid model (red line). In Fig. 5.2 Δ_u is the ultimate displacement, Δ_1 and Δ_2 are displacements related to material properties and to the state of degradation of the mortar joints at the pivot points. The values of Δ_1 and Δ_2 have been assumed in accordance with the proposed formulations of Sorrentino (Sorrentino, 2003) and are expressed in Eqn. 5.1 and Eqn. 5.2.

$$\Delta_1 = 0.05 \cdot \Delta_u \tag{5.1}$$

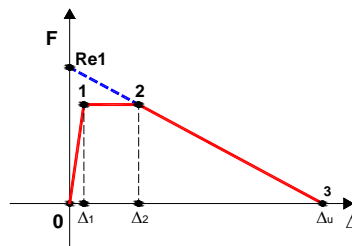$$\Delta_2 = 0.92 \cdot \Delta_1 + 0.21 \cdot \Delta_u \tag{5.2}$$

Figure 5.2 Simply supported wall (1DOF model): mid-height acceleration-displacement curve

5.3. Gaussian inputs

Gaussian impulse inputs in terms of displacement with duration T_1=1 s and T_2=2 s and variable maximum amplitudes have been used to perform dynamic analyses on the set of walls. 4 different values of the stiffness K_d of the spring at the top in the 2DOF model have been considered (K_d= 1000 KN/m, 100 KN/m, 50 KN/m and 10 KN/m). Fig. 5.3 shows the displacement time-histories of wall n.1 for Gaussian input with amplitude *D*=40 mm and T_1=1 s for the 1DOF model and 2DOF model: increasing the value of K_d, the response of the 2DOF model tends to reproduce well the response of

the 1DOF model, so that the top displacement s_2 becomes close to zero. Diminishing K_d the top displacement s_2 increases. The rotations q_1 and q_2, in opposition of phase in the 1DOF model, become more uncoupled and independent. The mid-height displacement s_1 increases passing from K_d=1000 KN/m to K_d=50 KN/m, but begins to decrease when K_d=10 KN/m. For that value of K_d the top displacement s_2 becomes larger than the mid-height displacement s_1 and s_2 and s_1 begin to be in phase.
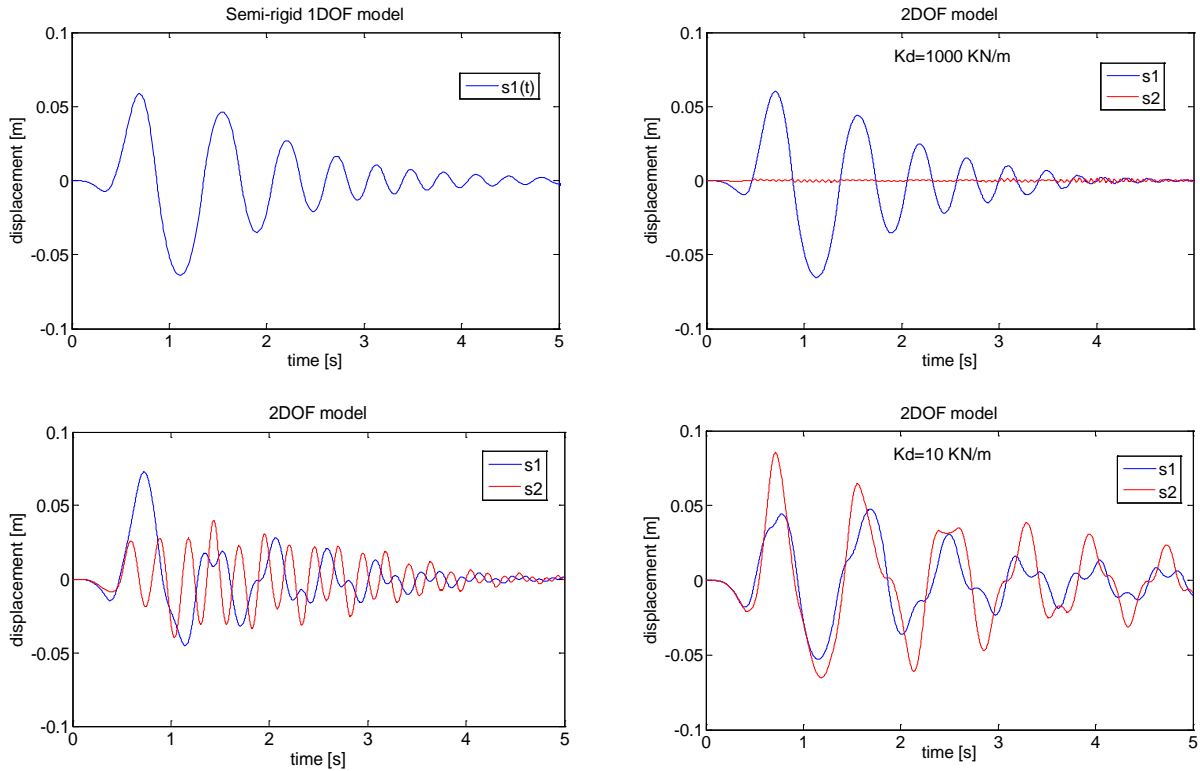

Figure 5.3 Wall n.1: displacement time-histories for 1DOF and 2DOF models with different values of K_d; s_1=mid-height displacement, s_2=top displacement; gaussian input with amplitude D=40 mm and duration T_1=1 s

Table 5.2. Gaussian input: maximum mid-height and top displacements s_1 and s_2; comparison between 1DOF and 2DOF results

Wall	Impulse duration	Impulse amplitude	1DOF	Maximum displacement $	\Delta	$max							
				2DOF							
				K_d=1000 KN/m		K_d=100 N/m		K_d=50 KN/m		K_d=10 N/m	
			s_1	s_1	s_2	s_1	s_2	s_1	s_2	s_1	s_2
		[m]	[m]	[m]	[m]	[m]	[m]	[m]	[m]	[m]	[m]
1	T_1=1 s	0,040	0,064	0,066	0,002	0,069	0,021	0,073	0,040	0,053	0,085
2	T_1=1 s	0,040	0,040	0,613	0,003	0,093	0,036	0,058	0,047	0,033	0,073
3	T_1=1 s	0,050	0,033	0,068	0,008	0,056	0,056	0,034	0,063	0,030	0,053

Table 5.2 shows the maximum displacements s_1 and s_2 of walls n.1, 2 and 3 for Gaussian impulse inputs with duration T_1=1 s and different amplitudes: the trend described for wall n.1 in Fig. 5.3 is confirmed. Increasing the value of K_d the top displacement s_2 becomes close to zero, while the mid-height displacement s_1 increases until a specific value of K_d and then diminishes, so that s_2 becomes greater than s_1. With a significant overburden load (wall n.3) s_1 decreases while K_d gets smaller. The trend for Gaussian inputs with T_2=2 s is similar to the one with T_1=1 s.

5.4. Recorded accelerogram inputs

6 recorded accelerograms have been assumed as input to perform dynamic analyses on the 3 walls. Table 5.3 describes the characteristics of the records.

Table 5.3. Recorded accelerograms used in the analyses

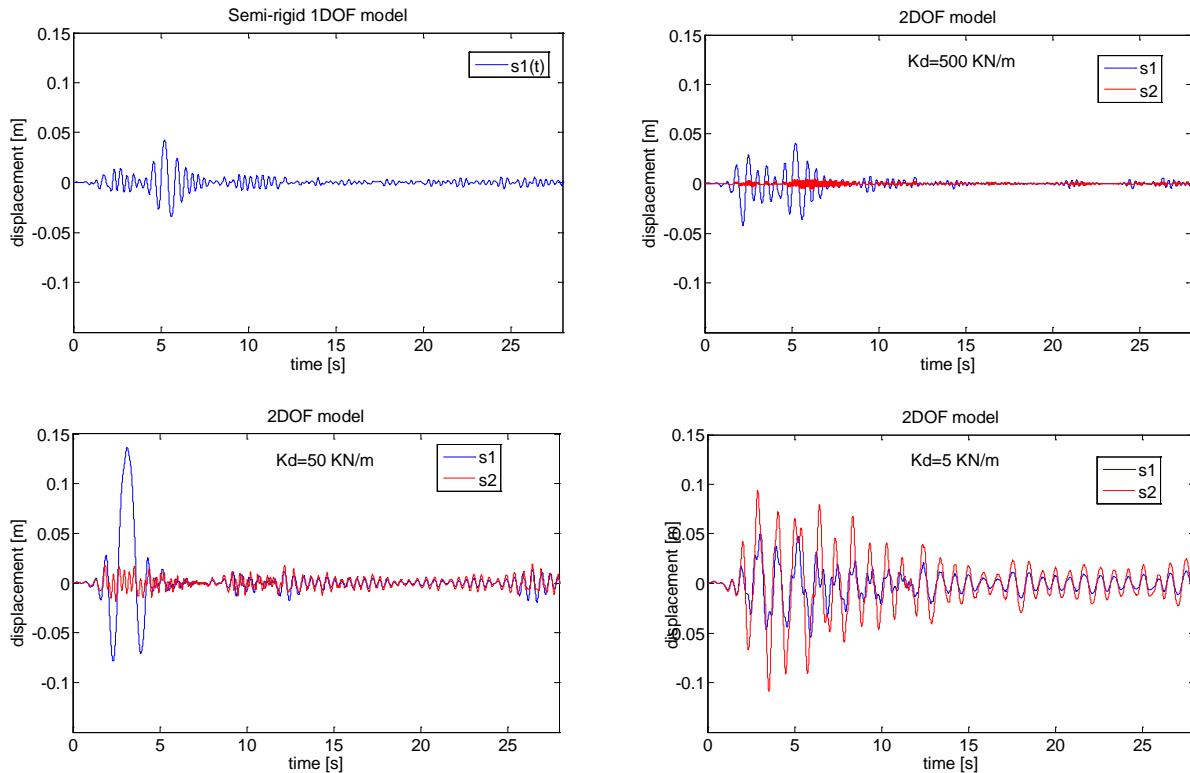| Event	Year	Station	Id.	Component	PGA
Imperial Valley	1940	El Centro	Elce	S00E	0.348 g
Friuli	1976	Tolmezzo	tolm	270	0.315 g
Irpinia	1980	Sturno	stur	270	0.358 g
Loma Prieta	1989	Capitola	loma	000	0.529 g
Northridge	1994	Sylmar Hospital	Sylm	360	0.843 g
Kobe	1995	KJMA	kjmh	000	0.821 g

Figure 5.4 Wall n.1: displacement time-histories for 1DOF and 2DOF models with different values of K_d; s_1=mid-height displacement, s_2=top displacement; El Centro recorded accelerogram scaled to 50% of PGA

Fig. 5.4 shows the displacement time-histories of wall n.1. for El Centro record, scaled at 50% of PGA, for the 1DOF model and for the 2DOF model: for the value of K_d =500 KN/m, the response of the 2DOF model tends to reproduce the response of the 1DOF model, even better than for Gaussian inputs. Diminishing K_d the top displacement s_2 increases and has a significant magnification for K_d=50 KN/m, when it becomes quite 3 times the value for K_d =500 KN/m. For K_d=5 KN/m the top displacement s_2 becomes greater than the mid-height displacement s_1.

Table 5.4. Recorded accelerograms: maximum mid-height and top displacements s_1 and s_2; comparison between 1DOF and 2DOF results

Wall 1		Maximum displacement |Δ|max						
		1DOF	**2DOF**					
Accelerogram	**% PGA**		K_d=500 KN/m		K_d=50 KN/m		K_d=5 K/m	
		s_1	s_1	s_2	s_1	s_2	s_1	s_2
		[m]	[m]	[m]	[m]	[m]	[m]	[m]
elce	50	0,043	0,043	0,004	0,137	0,019	0,050	0,109
tolm	100	0,094	0,094	0,004	0,114	0,036	0,048	0,095
stur	80	0,053	0,048	0,005	0,035	0,023	0,082	0,074
loma	50	0,031	0,034	0,004	0,039	0,026	0,056	0,078
sylm	35	0,045	0,047	0,005	0,057	0,028	0,077	0,082
kjmh	20	0,063	0,068	0,004	0,046	0,035	0,060	0,114

Table 5.4 shows the maximum displacements s_1 and s_2 of wall n.1 for recorded accelerogram inputs scaled at different percentage of PGA: the trend described in Fig. 5.4 is partially confirmed, even if it is less regular for different ground motions. Increasing the value of K_d the top displacement s_2 becomes close to zero; the mid-height displacement s_1 does not follow a common trend for all the records. With high values of K_d the collapse of the wall takes place because of excessive mid-height displacement demand as in the case of simply supported wall (1DOF). With small values of K_d, s_2 becomes greater than s_1 and collapse takes place for excessive top displacement demand, similarly to the parapet wall. Results obtained for wall n. 2 and n. 3 are similar to the ones obtained for wall n. 1.

5.5. Observations

An extension of the present study will be necessary to better investigate the influence of diaphragm flexibility on the out-of-plane behaviour of walls. It is anyway already possible to highlight that neglecting diaphragm flexibility can be either over conservative or can lead to a significant and dangerous underestimation of the displacement demand on the wall, depending on the characteristics of the input and of the wall. The flexibility of the diaphragms has in fact a strong influence on the displacement demand and appears to be an important parameter to be included in the dynamic analyses of out-of-plane behaviour of unreinforced masonry walls.

6. CONCLUSIONS

The present work is an attempt to extend some formulations and concepts proposed by other authors for the parapet wall and for the simply supported wall to the case of the out-of-plane bending of walls in buildings with flexible diaphragms. The results of dynamic analyses on a set of walls with Gaussian impulse or with recorded accelerogram inputs has been investigated: the stiffness of the diaphragm has a strong influence on the displacement demand of the walls, even if it seems that it is not possible to define a general rule to predict such demand without performing dynamic analyses. The hypotheses made in developing the model and the numerical algorithm need to be validated by experimental tests. Future developments could be the modelling of the inelastic behaviour of the spring at the top and the definition of a 3-degrees-of-freedom model that includes the in-plane walls.

REFERENCES

Doherty, K. (2000). An investigation of the weak links in the seismic load path of unreinforced masonry buildings. , PhD Thesis. Department of Civil and Environmental Engineering, The University of Adelaide.

Doherty, K., Griffith, M. C., Lam N. and Wilson, J. (2002). Displacement-based seismic analysis for out-of-plane bending of unreinforced masonry walls. *Earthquake Engineering and Structural Dynamics*, **31**, 833-850

Griffith, M. C., Magenes, G., Melis, G. and Picchi, L. (2003). Evaluation of out of plane stability of unreinforced masonry walls subjected to seismic excitation. *Journal of Earthquake Engineering*, **7:S1**, 141-169

Griffith, M. C., Lam , N. T. K., Wilson , J. L. and Doherty, K. (2004). Experimental investigation of Unreiforced Brick Masonry Walls in Flexure. *Journal of Structural Engineering ASCE.* **130:3**, 423-432.

Housner, G.W. (1963). The behavior of inverted pendulum structures during earthquakes, *Bulletin of the Seismological Society of America*, **53:2**, 403-417.

Lam , N. T. K., Griffith, M. , Wilson, J. and Doherty, K. (2003). Time–history analysis of URM walls in out-of-plane flexure. Engineering *Structures*, **25**, 743-754

Simsir, C.C. (2004). Influence of diaphragm flexibility on the out-of-plane dynamic response of unreinforced masonry walls. PhD Thesis, University of Illinois at Urbana Champagne, Illinois, USA.

Sorrentino, L. (2003). Dinamica di muri sollecitati fuori del piano come sistemi di corpi rigidi. PhD Thesis, Dottorato di Ricerca in Ingegneria delle Strutture – XVI Ciclo Università degli Studi di Roma "La Sapienza"

Sorrentino, L., Masiani, R. and Griffith, M.C. (2008). The vertical spanning strip wall as a coupled rocking rigid body assembly, *Structural Engineering and Mechanics*, **29:4**, 433-453